Acta Geotechnica
https://doi.org/10.1007/s11440-026-03092-5

RESEARCH PAPER

Optimal design of grouted anchor group using a newly developed pullout response theoretical analysis method considering group effect and the GWO algorithm

Shimin Zhu[1] · Hui Geng[1] · Changfu Chen[2] · Song Gao[2] · Kezhi Song[1] · Genbao Zhang[3]

Received: 16 October 2025 / Accepted: 17 May 2026

Abstract
The anchor group developed by a dense arrangement of grouted anchors has been widely employed in a variety of geotechnical reinforcement projects. Compared to a single anchor, the anchor group exhibits significantly more intricate load–displacement mechanisms due to the interaction between adjacent anchors (group effect), which brings great challenge to the bearing performance analysis and optimal design. In this paper, a theoretical approach for analyzing the pullout responses of the grouted anchor group was proposed by integrating load-transfer theory and shear deformation method. Herein, a generalized tri-linear bond-slip model was utilized to characterize the soil–grout interface nonlinear behaviors. The predicted pullout load–displacement responses and axial force distributions are generally in good agreement with the results from in-situ and laboratory pullout tests for both single anchor and anchor group, thereby confirming the efficacy and accuracy of the theoretical analysis method. Based on grey wolf optimization (GWO) algorithm, a novel optimal design method driven by the lowest cost was developed for the grouted anchor group. The discussion on an actual anti-floating anchorage engineering indicated that the GWO-based optimal design method provides excellent accuracy and fast convergence speed in searching for the best design parameters. Parametric studies were conducted to investigate the effects of some key design parameters on the bearing capacity of anchor group. The present work provides insights into the bearing performance evaluation of the grouted anchor group and facilitates the cost-effective optimal design.

Keywords Group effect · Grouted anchor · Optimal design · Pullout response · Theoretical analysis

1 Introduction

Ground anchors are equipped with the virtues of cost effectiveness, convenience of construction, minimal environmental disturbance, and superior bearing performance. The combination of these merits facilitates the extensive application of this technology in a variety of geotechnical engineering projects, such as slopes [27, 37], foundation pits [23], tunnels [39], and underground structure anti-floating [18]. In China, the total length of the anchors merely utilized for deep excavation supporting amounts to 10 billion meters each year [8]. The external pullout load borne by the anchor is generally transferred to the surrounding stable geomaterial mass via the soil–grout interface shear resistance, thereby achieving the objective of supporting the engineering structure and reinforcing the unstable geomaterial mass [4, 20, 43]. The bearing capacity of a single anchor is limited and usually insufficient to satisfy the requirements of the engineering structure. The dense arrangement of anchors to form the anchor group system is inevitable for enhancing the bearing capacity, especially in cases where the soil quality is poor and the reinforcement area is comparatively large. However, the adjacent anchors within the anchor group will interact with each other due to stress superposition. This phenomenon, known as group effect, has been proven to cause a loss in

✉ Shimin Zhu
smzhu@ldu.edu.cn

[1] School of Hydraulic and Civil Engineering, Ludong University, Yantai 264025, Shandong, China

[2] College of Civil Engineering, Hunan University, Changsha 410082, Hunan, China

[3] College of Civil Engineering, Hunan City University, Yiyang 413000, Hunan, China

Published online: 09 June 2026

the bearing efficiency of the ground anchors [12, 15, 19]. Therefore, the anchor group exhibits significantly more intricate load–displacement mechanisms in comparison to a single anchor, and its bearing capacity cannot be deduced as the sum of the bearing capacities of all individual anchors.

There is generally a large ratio of anchorage length to diameter for grouted anchors. When the anchor is subjected to pullout load, the axial force and the soil–grout interface shear stress will both distribute non-linearly along the anchorage segment due to the tensile deformation of the anchor body [33, 52]. The load-transfer behavior of the anchors can exert a significant influence on their pullout capacity. At present, relatively abundant studies focus on the load-transfer behavior or the pullout capacity of a single anchor. A multitude of in-situ pullout tests [22, 34, 47, 48] and laboratory pullout tests [6, 38, 45, 51] have been conducted to ascertain the pullout capacities or the stress distributions of different structural types of anchors under various loading or construction conditions. Additionally, some scholars proposed or selected different forms of bond-slip models to characterize the soil–anchor interface nonlinear mechanical behaviors. On this basis, theoretical analysis methods for the pullout responses of ground anchors under various working conditions were developed by the utilization of load-transfer theory [13, 24, 33, 36, 52]. These studies provided profound insights into the safety performance assessment and the design of the anchorage structure.

The group effect will inevitably lead to a reduction in the bearing capacity of the anchor group. This phenomenon is analogous to that of piles [10, 30, 42, 44]. Hong et al. [14] found that the bearing efficiency coefficient of the anchor group embedded in sandy soil could attain 100% only when the spacing distance between adjacent anchors reached 16 times the diameter of the anchor, whereas it required 24 times the diameter if the interface roughness increased from 0 to 0.335. The test results from Akis et al. [1] indicated that the bearing capacity of the anchor group embedded in clay would decrease by approximately 16.8% once the spacing distance was reduced to twice the diameter of the anchor, and the bearing efficiency coefficient could attain 100% only when the spacing distance exceeded 6 times the diameter. In addition, Chen et al. [5], Li et al. [21], and Wang and Zhang [40] investigated the failure modes and bearing capacities of the anchor group through in-situ pullout tests, laboratory model tests, and numerical simulations. There are also several achievements relevant to theoretical modeling. Hu and Chen [15] proposed a theoretical approach for calculating the pullout displacement at the head of the anchor group. Pang et al. [28] discussed the influence of spacing distance on the stress distribution of an individual anchor within the recyclable anchor group through the Kelvin solution-based calculation formula. Noteworthy that these methods cannot be used to determine the bearing capacity of the anchor group. Ozturk [26] proposed a neural network-based method for predicting the bearing capacity of tension anchors, which considered the group effect but could not be used to analyze stress distributions. To summarize, there is still a lack of theoretical analysis methods capable of simultaneously predicting the bearing capacity and the stress distributions of anchor group.

The issue of engineering cost minimization while adhering to established design requirements is of great concern for engineers. Since the twenty-first century, artificial intelligence optimization algorithms have been developing rapidly, resulting in the emergence of numerous efficient and stable global optimization algorithms [31]. In recent years, some intelligent algorithms have been successfully incorporated into the optimal design of various geotechnical engineering structures, such as piles [2, 29], composite foundation [3, 11], and slope support [16]. The design parameters of grouted anchor group include anchor diameter d, anchorage length L_a, free length L_f, spacing distance between adjacent anchors D_s, diameter of rebar or steel strand d_r, etc. It is extremely challenging to determine a set of values for the design parameters that can yield the lowest cost or the best bearing performance, given the many design parameters involved. Therefore, the employment of intelligent optimization algorithms is imperative to address this issue. Noteworthy that the development of an efficient and accurate theoretical method to calculate the bearing capacity of the anchor group is an essential precondition for the optimal design. However, no relevant studies are available in the reported works.

In this paper, a theoretical approach for analyzing the pullout behaviors of the grouted anchor group was developed by integrating load-transfer theory and shear deformation method. The pullout displacement of the anchor was specially divided into two parts, including the soil–grout interface shear displacement and the shear deformation of the surrounding soil. A generalized tri-linear bond-slip model was employed to describe the soil–grout interface nonlinear mechanical behavior. The results from four separate in-situ and laboratory pullout tests of the single anchor and the anchor group were utilized to verify the proposed theoretical method. The predicted pullout load–displacement responses and axial force distributions were compared with the testing results. A new optimal design method for the grouted anchor group was introduced based on the GWO algorithm. Herein, the total cost was defined as the objective function, and the bearing capacity and the construction requirements were stipulated as boundary conditions. The optimal design for anti-floating anchor group was discussed based on an actual engineering case.

Parametric studies were conducted to determine the effects of some key design parameters on the bearing capacity of the grouted anchor group.

2 Load–displacement responses of grouted anchor group

There is no apparent relationship between the pullout capacity or soil–anchor interface shear strength and the ground pressure for grouted anchors due to the soil stress release around the hole after drilling [35, 46]. It can thus be inferred that the pullout capacity of grouted anchor is basically independent of its layout direction. To facilitate the visualization of the displacement patterns of anchors and the surrounding soils, the anti-floating anchor group arranged along the vertical direction were analyzed as the example, as illustrated in Fig. 1. The failure of grouted anchors usually occurs at the soil–grout interface, particularly in the case of anchors embedded in clay. The anchor and its surrounding soil will exhibit relative displacement or movement when the anchor is subjected to pullout load. The shear stress present at the soil–grout interface will further cause shear deformation in the surrounding soil. Hence, the pullout displacement of the anchor s is comprised of the following two parts:

$$s = s_{a} + s_{s} \tag{1}$$

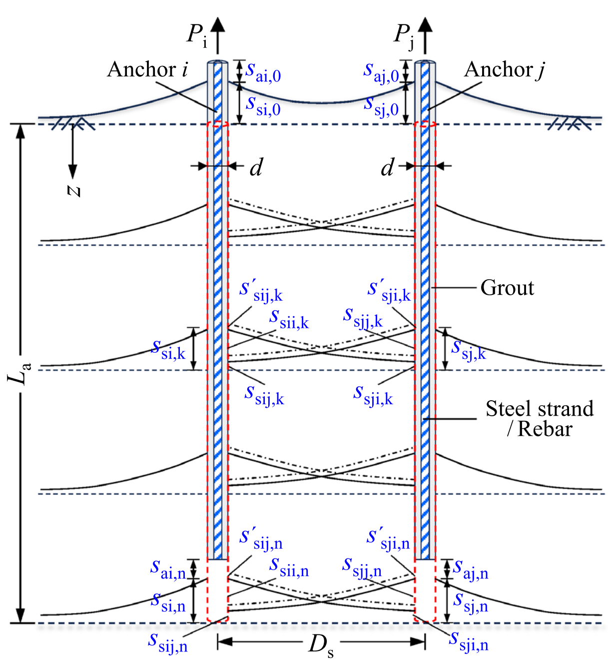

Fig. 1 Displacement patterns of the adjacent anchors and the surrounding soil in anchor group

where s_a is the soil–grout interface shear displacement; s_s is the shear deformation of the surrounding soil.

It is assumed that the grouted anchor group consists of m anchors, and all anchors are equipped with the same anchorage length L_a, diameter d, and spacing distance D_s. Two adjacent anchors, designated as i and j, were selected for analysis. Figure 2 shows the displacement composition for a micro-section of anchors i and j. The soil shear deformation surrounding anchor i can be categorized into three components [15], as delineated by Eq. (2). This aspect is similar to that of the pile group [10].

$$s_{si} = s_{sii} + s_{sij} - s'_{sij} \tag{2}$$

where s_{si} represents the soil shear deformation surrounding anchor i; s_{sii} represents the soil shear deformation caused by the pullout load P_i subjected to anchor i; s_{sij} represents the additional soil shear deformation around anchor i caused by pullout load P_j subjected to anchor j; s'_{sij} represents the reduction in soil shear displacement surrounding anchor i due to the reinforcement effect of anchor j in unload state.

3 Theoretical analysis method for the pullout behaviors of grouted anchor group

3.1 Basic assumptions

Two difficulties are hindering the theoretical analysis of the pullout responses of the grouted anchor group. Firstly, the soil–anchor interface generally exhibits significant nonlinear mechanical behaviors, so the utilization of an interface nonlinear mechanical model is essential for the characterization. Secondly, the adjacent anchors will interact with each other due to the superposition of stress, that is, the group effect. Therefore, the following assumptions were stipulated to facilitate the process of the theoretical analysis.

(a) The geometric design parameters and materials for all anchors within the grouted anchor group are the same, including anchorage length, free segment length, diameter, spacing distance, grouting material, rebar, etc.

(b) The anchor body should basically be in elastic state, except in cases where the pullout load is very large and exceeds its yield point. The plastic deformation of the surrounding soil may occur in response to the interface shear stress, but its contribution to the total pullout displacement is relatively minor. The incorporation of material plasticity would render

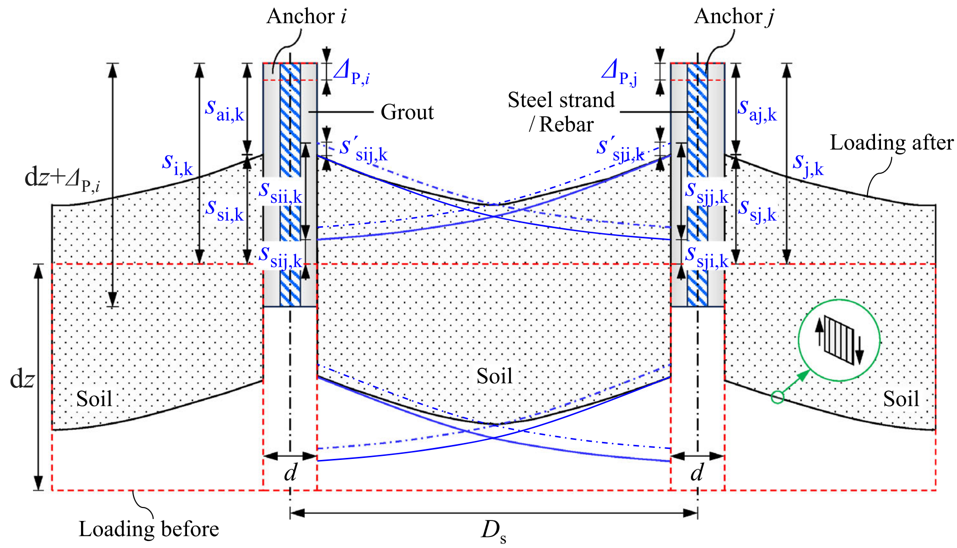

Fig. 2 Displacement composition for a micro-section of anchors i and j

theoretical modelling infeasible. Hence, the grout and its surrounding soil were assumed to be in elastic state, and their mechanical responses obey Hooke's law.

(c) The shear/bond strength of the steel rebar-grout interface is considerably higher than that of the soil–grout interface, so the failure of the grouted anchor generally occurs at the soil–grout interface. Therefore, the grout and steel rebar were considered as an entity to simplify the modeling process. A generalized tri-linear interface shear model was employed to characterize the nonlinear behaviors over the soil–grout interface.

(d) When analyzing the pullout responses of a specific anchor within the anchor group, the consideration of group effect is limited to the adjacent anchors around the designated anchor. The anchors that are spaced apart by one or more anchors from the selected anchor are disregarded due to the shielding of the adjacent anchors.

(e) It is hypothesized that the ratio of the pullout load applied to each anchor remains constant during the entire loading process. This relationship can be expressed as:

$$P_1 = \xi_2 \cdot P_2 = \cdots = \xi_j \cdot P_j = \cdots = \xi_m \cdot P_m \tag{3}$$

where ξ_j is the proportional coefficient between the pullout load borne by the first and j^{th} anchors.

3.2 Calculation of the soil shear deformation around the anchor

Similar to pile foundations [32], the soil shear deformation $s_{sii}(z, r_i)$ at a given depth z induced by the soil–grout interface shear stress $\tau_i(z)$ of anchor i can be calculated through the application of shear displacement method. It is expressed as:

$$s_{sii}(z, r_i) = \begin{cases} \dfrac{\tau_i(z) r_0}{G_s} \ln\left(\dfrac{r_m}{r_i}\right), & r_i < r_m \\ 0, & r_i \geq r_m \end{cases} \tag{4}$$

where r_0 represents the radius of the anchor; G_s represents the shear modulus of the surrounding soil, $G_s = \frac{E_s}{2(1+\mu)}$; μ represents Poisson's ratio of the soil; E_s represents Young's modulus of the soil; r_i represents the distance from the center of anchor i; r_m represents the influence range of interface shear stress, which can be estimated according to Eq. (5).

$$r_m = 2.5 \rho l_a (1 - \mu) \tag{5}$$

where ρ is the non-uniformity coefficient, representing the ratio of the soil shear modulus in the middle part of the anchorage segment to that of the bottom part; l_a is the anchorage length.

In reference to Eq. (4), the soil shear deformation $s_{sii}(z, r_0)$ along the surface of anchor i caused by interface shear stress $\tau_i(z)$ is derived as:

$$s_{\text{sii}}(z) = \frac{\tau_{\text{i}}(z) r_0}{G_{\text{s}}} \ln\left(\frac{r_{\text{m}}}{r_0}\right) \tag{6}$$

The interface shear stress $\tau_{\text{i}}(z)$ of anchor i is transferred radially outward. Based on the stress equilibrium condition, the movement of $\tau_{\text{i}}(z)$ to the position of the adjacent anchor j at the same depth will result in the following shear stress value, denoted by $\tau_{\text{ji}}(z)$.

$$\tau_{\text{ji}}(z) = \frac{\tau_{\text{i}}(z) r_0}{D_{\text{s}}} \tag{7}$$

where D_{s} is the spacing distance between anchor i and anchor j.

As illustrated in Fig. 3, the shear stress $\tau_{\text{ji}}(z)$ at the surface of anchor j is oriented upwards, which is consistent with the direction of the pullout load P_{j}, but opposite to the direction of the interface shear stress $\tau_{\text{j}}(z)$. Hence, the shear stress $\tau_{\text{ji}}(z)$ originated from the anchor i can be regarded as the additional load applied to the anchor j. It may be the main reason for the emergence of the group effect. In the event that the soil around anchor i undergoes shear deformation due to the application of pullout load P_{i}, the existence of the adjacent anchor j will impede this trend. This phenomenon is referred to as the reinforcement or blockage effect [15]. The reduction of soil shear deformation $s'_{\text{sij}}(z)$ around anchor i is primarily attributable to the reaction force of $\tau_{\text{ji}}(z)$. The substitution of Eq. (7) into Eq. (6) can yield the value of $s'_{\text{sij}}(z)$.

$$s'_{\text{sij}}(z) = \begin{cases} \dfrac{\tau_{\text{i}}(z) r_0^2}{G_{\text{s}} D_{\text{s}}} \ln \dfrac{r_{\text{m}}}{D_{\text{s}}}, & D_{\text{s}} < r_{\text{m}} \\ 0, & D_{\text{s}} \geq r_{\text{m}} \end{cases} \tag{8}$$

When the pullout load P_{j} is exerted on anchor j, the resultant interface shear stress $\tau_{\text{j}}(z)$ will cause additional soil shear deformation $s_{\text{ij}}(z)$ around the anchor i, which can be determined by Eq. (9).

$$s_{\text{sij}}(z) = \begin{cases} \dfrac{\tau_{\text{j}}(z) r_0}{G_{\text{s}}} \ln \dfrac{r_{\text{m}}}{D_{\text{s}}}, \ D_{\text{s}} < r_{\text{m}} \\ 0, \ D_{\text{s}} \geq r_{\text{m}} \end{cases} \tag{9}$$

It can be deduced that $s_{\text{sij}}(z)$ and $s_{\text{sjj}}(z)$ satisfy the following relationship:

$$s_{\text{sij}}(z) = \psi_{\text{ij}} \cdot s_{\text{sjj}}(z) \tag{10}$$

where ψ_{ij} denotes the influence coefficient of soil shear deformation, which can be calculated by Eq. (11).

$$\psi_{\text{ij}} = \begin{cases} \dfrac{\ln r_{\text{m}} - \ln D_{\text{s}}}{\ln r_{\text{m}} - \ln r_0}, \ D_{\text{s}} < r_{\text{m}} \\ 0, \ D_{\text{s}} \geq r_{\text{m}} \end{cases} \tag{11}$$

The total soil shear deformation $s_{\text{si}}(z)$ around anchor i can be obtained by substituting Eqs. (6), (8), and (9) into Eq. (2). Based on Assumption (d), $s_{\text{sij}}(z)$ and $s'_{\text{sij}}(z)$ of the anchor i caused by all adjacent anchors should be aggregated when calculating $s_{\text{si}}(z)$, as shown in Eq. (12).

$$\begin{aligned} s_{\text{si}}(z) &= s_{\text{sii}}(z) + \sum_{j=1, j\neq i}^{m} s_{\text{sij}}(z) - \sum_{j=1, j\neq i}^{m} s'_{\text{sij}}(z) \\ &= \frac{\tau_{\text{i}}(z) r_0}{G_{\text{s}}} \ln\left(\frac{r_{\text{m}}}{r_0}\right) + \sum_{j=1, j\neq i}^{m} \frac{\tau_{\text{j}}(z) r_0}{G_{\text{s}}} \ln \frac{r_{\text{m}}}{D_{\text{s}}} \\ &\quad - \sum_{j=1, j\neq i}^{m} \frac{\tau_{\text{i}}(z) r_0^2}{G_{\text{s}} D_{\text{s}}} \ln \frac{r_{\text{m}}}{D_{\text{s}}} \end{aligned} \tag{12}$$

where m represents the number of the designated anchor i and its adjacent anchors; D_{s} represents the spacing distance between adjacent anchors.

It can be concluded from Eq. (12) that the pivotal factor in calculating $s_{\text{si}}(z)$ is to determine the soil–grout interface shear stress for each individual anchor within the anchor group. The load-transfer method would be employed in the subsequent theoretical analysis.

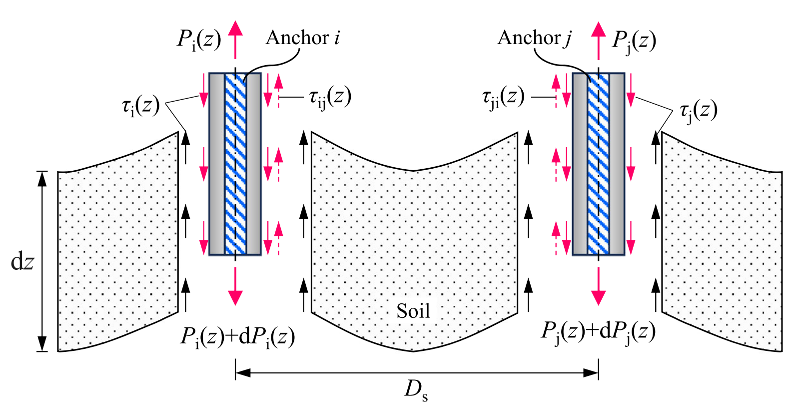

Fig. 3 Stress distribution in an elementary length dz of the anchor i and anchor j

3.3 Calculation of the soil–anchor interface shear displacement

3.3.1 Basic equations for the load-transfer analysis

The elementary segments of anchors i and j at a depth of z were selected for analysis (Fig. 3). According to Assumption (b), the tensile strain $\varepsilon_{\mathrm{i}}(z)$ for the elementary segment of anchor i can be expressed as:

$$\varepsilon_{\mathrm{i}}(z) = \frac{P_{\mathrm{i}}(z)}{E_{\mathrm{rg}}A_{\mathrm{a}}} \tag{13}$$

where $P_{\mathrm{i}}(z)$ is the axial tensile force of anchor i at depth z; A_{a} is the cross-sectional area of the anchors; E_{rg} is the composite elastic modulus of grout and rebar, which can be determined by the following equation.

$$E_{\mathrm{rg}} = \frac{E_{\mathrm{g}}A_{\mathrm{g}} + E_{\mathrm{r}}A_{\mathrm{r}}}{A_{\mathrm{a}}} \tag{14}$$

where E_{g} and E_{r} are elastic moduli of the grout and rebar, respectively; A_{g} and A_{r} are cross-sectional areas of the grout and rebar, respectively.

The axial tensile deformation of the elementary anchor segment is equivalent to the difference in interface shear displacement at its two ends. The relationship between the axial tensile strain $\varepsilon_{\mathrm{i}}(z)$ of the anchor and the interface shear stress $s_{\mathrm{ai}}(z)$ can thus be derived:

$$\varepsilon_{\mathrm{i}}(z) = -\frac{ds_{\mathrm{ai}}(z)}{dz} \tag{15}$$

It is hypothesized that the shear stress transmitted from anchor j is uniformly distributed along the cylindrical surface of anchor i. Hence, Eq. (16) can be obtained:

$$d \cdot \tau_{\mathrm{ij}} = u_{\mathrm{p}} \cdot \tau''_{\mathrm{ij}} \tag{16}$$

where d and u_{p} represents the diameter and perimeter of the anchor; τ_{ij} represents the shear stress transferred from anchor j to anchor i; τ''_{ij} represents the equivalent shear stress of τ_{ij} on the cylindrical surface of anchor i.

The equivalent shear stress τ''_{ij} can be rewritten as the following form by combining Eqs. (7) and (16):

$$\tau''_{\mathrm{ij}} = \frac{\tau_{\mathrm{j}}(z)r_0}{\pi D_{\mathrm{s}}} \tag{17}$$

As illustrated in Fig. 3, force equilibrium equation of the elementary anchor segment can be deduced as:

$$\frac{dP_{\mathrm{i}}(z)}{dz} + u_{\mathrm{p}}\left[\tau_{\mathrm{i}}(z) - \sum_{j=1, j\neq i}^{m} \frac{\tau_{\mathrm{j}}(z)r_0}{\pi D_{\mathrm{s}}}\right] = 0 \tag{18}$$

By combining Eqs. (13), (15), and (18), the load-transfer governing equation for each anchor in the anchor group is obtained:

$$\frac{d^2 s_{\mathrm{ai}}(z)}{dz^2} - \frac{u_{\mathrm{p}}}{E_{\mathrm{rg}}A_{\mathrm{a}}}\left[\tau_{\mathrm{i}}(z) - \sum_{j=1, j\neq i}^{m} \frac{\tau_{\mathrm{j}}(z)r_0}{\pi D_{\mathrm{s}}}\right] = 0 \tag{19}$$

The solution to the governing equation depends largely on the selection of a suitable mechanical model to characterize the relationship between interface shear stress and interface shear displacement.

3.3.2 A generalized tri-linear bond-slip model for describing the soil–grout interface nonlinear behaviors

The tri-linear bond-slip model has been extensively employed in the load-transfer theoretical analysis for ground anchors and piles due to its multiple virtues, including the ability to describe the softening or hardening soil–structure interface nonlinear behaviors, fewer parameters that need to be calibrated [17, 24, 33, 49]. The graphical form of the generalized tri-linear bond-slip model is depicted in Fig. 4, and its function expression for the relationship between interface shear stress τ and interface shear displacement is:

$$\tau(s) = \begin{cases} k_e s, & 0 \leq s \leq s_e \\ \tau_f + k_p(s - s_e), & s_e < s \leq s_p \\ (1-\eta)\tau_f, & s > s_p \end{cases} \tag{20}$$

where s_{e} denotes ultimate interface elastic shear displacement; s_{p} denotes ultimate interface plastic shear displacement; τ_{f} denotes peak interface shear strength; k_{e} denotes interface elastic shear stiffness; k_{p} denotes interface plastic shear stiffness; η denotes interface softening coefficient, $\eta = (\tau_{\mathrm{f}} - \tau_{\mathrm{r}})/\tau_{\mathrm{f}}$; τ_{r} denotes residual interface shear strength.

As shown in Fig. 4, the generalized tri-linear bond-slip model exhibits three different forms based on the value of interface softening coefficient η, including softening

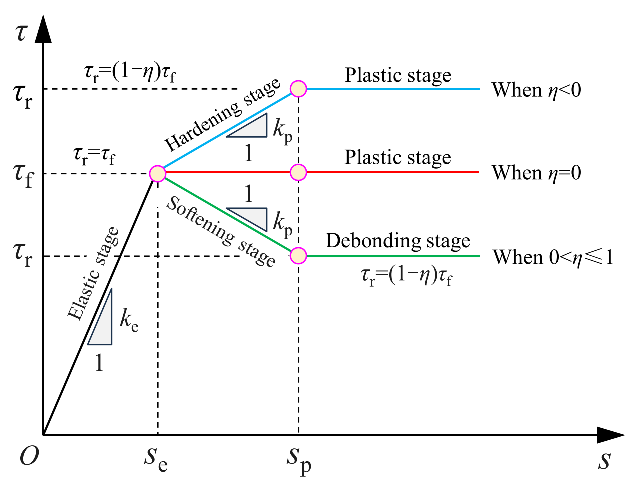

Fig. 4 Graphical form of the generalized tri-linear bond-slip model

pattern ($0 < \eta \leq 1$), hardening pattern ($\eta < 0$), and idealized elastoplastic pattern ($\eta = 1$). More details can be found in Zhu et al. [49].

3.4 Finite difference solution of the load–displacement response

The load-transfer governing equation of anchor group can be completed by substituting Eq. (20) into Eq. (19). However, as previously mentioned, the adjacent anchors will exert cross-influences on each other's pullout behavior. This phenomenon is also implicitly contained in Eq. (19). It is nearly impossible to obtain the analytical solution for the load–displacement response of the anchor group. Consequently, the finite difference method would be utilized to derive the solution. The steps are presented below.

Step (1): The anchorage segments for all anchors are uniformly divided into n units along the axial direction. According to Assumption (a), all anchors within the anchor group are equipped with the same anchorage length L_a, so the lengths for all anchor units ΔL_a are equal to L_a/n. There are all $n + 1$ nodes for each anchor. Anchor i is taken as the example, the $n + 1$ nodes of which are sequentially numbered $z_{i,0}$, $z_{i,1}$, …, $z_{i,n}$ from the beginning to the end of the anchorage segment. The value of n can be designated according to computational precision.

Step (2): The interface shear displacement at the end of the anchor i (node $z_{i,n}$) is assigned as a value of $s_{ai,n}$. Meanwhile, the interface shear displacements $s_{aj,n}^{(1)}$ ($j = 1$, …, m, $j \neq i$) at the end of other anchors j is assumed to be $s_{ai,n}$ in the first round of iterative computation. The superscript in "$s_{aj,n}^{(1)}$" denotes the number of iterative computations. The interface shear stress $\tau_{k,n}$ at node $z_{k,n}$ ($k = 1$, …, m) for all anchors in the anchor group can be calculated by Eq. (20). The shear stresses $\tau_{ij,n}$ ($j = 1$, …, m, $j \neq i$) transferred from anchors j to anchor i is further determined by Eq. (7). The soil shear deformation $s_{si,n}$ around anchor i is obtained by Eq. (12). Noteworthy that the axial tensile forces for each anchor in the anchor group are zero at the end of the anchorage segment. In this way, the axial forces $P_{k,n}$, interface shear stresses $\tau_{k,n}$, interface shear displacements $s_{ak,n}$, and soil shear deformations $s_{sk,n}$ for all anchors at node $z_{k,n}$ ($k = 1$, …, m) can be determined.

Step (3): For node $z_{i,n-1}$, the axial force $P_{i,n-1}$ of anchor i can be derived based on the differential form of Eq. (18), as shown below.

$$P_{i,n-1} = u_p\left(\tau_{i,n} - \sum_{j=1,j\neq i}^{m} \frac{\tau_{j,n} \cdot r_0}{\pi D_s}\right)\Delta L_a \tag{21}$$

Combing Eqs. (13) and (15), the interface shear displacement $s_{ai,n-1}$ at node $z_{i,n-1}$ is determined:

$$s_{ai,n-1} = s_{ai,n} + \varepsilon_{i,n-1} \cdot \Delta L_a = s_{ai,n} + \frac{P_{i,n-1}}{E_{rb}A_a}\Delta L_a \tag{22}$$

where $\varepsilon_{i,n-1}$ represents the axial tensile strain of anchor i at node $z_{i,n-1}$.

The interface shear stress $\tau_{i,n-1}$ at node $z_{i,n-1}$ is calculated by Eq. (20). In a similar way, the axial force $P_{j,n-1}$, interface shear displacement $s_{ai,n-1}$, and interface shear stress $\tau_{j,n-1}$ for the other anchors at node $z_{j,n-1}$ ($j = 1$, …, m, $j \neq i$) can also be obtained. Subsequently, the soil shear deformations $s_{sk,n-1}$ for all anchors within the anchor group at node $z_{k,n-1}$ ($k = 1$, …, m) are determined by Eq. (12).

Step (4): The load-transfer governing equation (Eq. 19) is rewritten as the difference form at node $z_{i,n-1}$. The interface shear stress $s_{ai,n-2}$ of anchor i at node $z_{i,n-2}$ can thus be derived:

$$\begin{aligned} s_{ai,n-2} &= 2s_{ai,n-1} - s_{ai,n} \\ &\quad + \frac{u_p}{E_{rg}A_a}\left(\tau_{i,n-1} - \sum_{j=1,j\neq i}^{m} \frac{\tau_{j,n-1} \cdot r_0}{\pi D_{s,ij}}\right)\Delta L_a^2 \end{aligned} \tag{23}$$

The axial force $P_{i,n-2}$ at node $z_{i,n-2}$ is determined by Eq. (18):

$$P_{i,n-2} = P_{i,n-1} + u_p\left(\tau_{i,n-1} - \sum_{j=1,j\neq i}^{m} \frac{\tau_{j,n-1} \cdot r_0}{\pi D_{s,ij}}\right)\Delta L_a \tag{24}$$

The interface shear stress $\tau_{i,n-2}$ at node $z_{i,n-2}$ is calculated by Eq. (20). Analogously, the axial force $P_{j,n-2}$, interface shear displacement $s_{ai,n-2}$, and interface shear stress $\tau_{j,n-2}$ for the other anchors at node $z_{j,n-2}$ ($j = 1$, …, m, $j \neq i$) can also be obtained. The soil shear deformations $s_{sk,n-2}$ for all anchors at node $z_{k,n-2}$ ($k = 1$, …, m) are determined by Eq. (12). In a similar manner to this step, the load–displacement responses for all anchors at the remaining nodes can be determined successively.

Step (5): In some special cases, such as anti-floating anchor group, the proportional coefficients ξ_j ($j = 2$, …, m) between the pullout load borne by the first and the other anchors are all equal to 1. In other words, the pullout loads and the pullout displacements at anchor heads for all anchors are the same within the anchor group. The boundary conditions are:

$$\begin{cases} P_1 = P_2 = \cdots = P_m \\ s_{1,0} = s_{2,0} = \cdots = s_{m,0} \end{cases} \tag{25}$$

Iterative calculation is not necessary in this case because all anchors exhibit the same load–displacement responses. However, iterative calculation is required if $\xi_j \neq 1$. The results should satisfy the boundary condition shown in Eq. (3) when all interface shear displacements $s_{aj,n}$ ($j = 1$,

…, m, $j \neq i$) converge to the corresponding accurate values. Equation (26) is employed to narrow the scope in which the precise value of $s_{\mathrm{aj,n}}$ is located.

$$\begin{cases} s_{\mathrm{aj,n,max}}^{(g)}=s_{\mathrm{aj,n}}^{(g-1)},\ s_{\mathrm{aj,n,min}}^{(g)}=s_{\mathrm{aj,n,min}}^{(g-1)}, & \text{if } P_{\mathrm{j}}^{(g-1)} > \xi_{\mathrm{j}} \cdot P_{\mathrm{i}}^{(g-1)} \\ s_{\mathrm{aj,n,max}}^{(g)}=s_{\mathrm{aj,n,max}}^{(g-1)},\ s_{\mathrm{aj,n,min}}^{(g)}=s_{\mathrm{aj,n}}^{(g-1)}, & \text{if } P_{\mathrm{j}}^{(g-1)} < \xi_{\mathrm{j}} \cdot P_{\mathrm{i}}^{(g-1)} \end{cases} \tag{26}$$

where the superscript "g" represents the number of iterations.

In the g^{th} round of iterative computation, the interface shear displacements $s_{\mathrm{aj,n}}^{(\mathrm{g})}$ at the end of anchors j (j = 1, …, m, $j \neq i$) are reassigned as:

$$s_{\mathrm{aj,n}}^{(g)} = \frac{1}{2}\left[s_{\mathrm{aj,n,max}}^{(g)} + s_{\mathrm{aj,n,min}}^{(g)}\right] \tag{27}$$

Repeating steps (2) to (4) until the specified calculation accuracy δ_{r} is achieved.

$$\sum_{j=1,j\neq i}^{m} \left|P_{\mathrm{j}}^{(k)} - \xi_{\mathrm{j}} \cdot P_{\mathrm{i}}^{(k)}\right| \leq \delta_r \tag{28}$$

Step (6): The interface shear displacement $s_{\mathrm{ai,n}}$ at the end of the anchor i (node $z_{\mathrm{i,n}}$) is reassigned a new value. Subsequently, the stress and displacement distributions for each individual anchor within the anchor group under different pullout loads can thus be obtained by repeating steps (2) to (5). Equation (29) can be utilized to calculate the pullout displacements at the heads of each anchor.

$$s_{\mathrm{hi}} = s_{\mathrm{ai,0}} + s_{\mathrm{si,0}} + \frac{P_{\mathrm{i}} L_{\mathrm{f}}}{E_{\mathrm{r}} A_{\mathrm{r}}} \tag{29}$$

where s_{hi} denotes the pullout displacement at the head of anchor i; $s_{\mathrm{ai,0}}$ and $s_{\mathrm{si,0}}$ denote the interface shear displacement and the soil shear deformation at the beginning of anchorage segment of anchor i, respectively; L_{f} denotes the free length of anchor i.

The pullout load–displacement curves for each individual anchor within the anchor group can be obtained by accomplishing the aforementioned steps. The maximum pullout load shown in the load–displacement curve approximately corresponds to the pullout capacity.

The finite difference solution for the pullout response of anchor group essentially falls within the category of theoretical solutions. This is because the derivation process merely involves theoretical methodologies. In comparison with the finite element model (FEM), the developed theoretical analysis method exhibits a significantly higher computational efficiency. It facilitates the application of this theoretical method in the subsequent optimal design of anchor group. The utilization of finite difference method in the theoretical modeling can also offer the potential for analyzing the pullout performance of the anchor group in layer soils. Specifically, segmented analysis is conducted based on the soil distribution. All junctions between different soil layers should be defined as the computational segmentation nodes. Noteworthy that the interface model parameters and the shear moduli of each layer of soil need to be substituted into the corresponding theoretical calculation segments in the analysis process. The procedures can be referred to that of a single anchor [50].

The assumptions delineated in Sub-Sect. 3.1 impose some limitations on the use of the proposed theoretical analysis model. In certain instances, this theoretical method will exhibit diminished calculation accuracy, or become inapplicable. For example, (1) the pullout load is very large and exceeds the yield stress of grout body; (2) ignoring the plastic shear deformation of the surrounding soil will lead to an underestimation of the total pullout displacement of the anchor group, particularly in cases where the interface shear stress is relatively large; (3) the lengths of each anchor in the group are not uniform; (4) the steel rebars or strands are separated from the grout due to the extremely large interface shear stress, particularly for the case of anchors embedded in hard soil or rock.

4 Verification of the theoretical analysis method through in-situ and laboratory pullout tests

4.1 Case 1: In-situ pullout test on the large-diameter cemented soil anchor group

Chen et al. [5] conducted in-situ pullout tests on a single large-diameter cemented soil anchor and anchor group that is adopted in foundation pit. The anchors were all 0.5 m in diameter, 15 m in anchorage length, and 5 m in free length. The steel strands with dimension of 2φ17.8 mm were utilized. In the testing anchor group, each row was equipped with three anchors with horizontal spacing of 2 m. The three anchors in the anchor group were loaded simultaneously using three hydraulic jacks. The pullout loads applied to the heads of all anchors remained equivalent during the entire loading process, and they were divided into four levels, including 160kN, 240kN, 320kN, and 400kN. The anchorage segment was mainly located in the medium sand interbedded with silt. The mechanical parameters of the tested soil were summarized as: Young's modulus E_{s} = 9 MPa, Poisson's ratio v_{s} = 0.3, cohesion c = 3 kPa, internal friction angle φ = 20°, and shear modulus G_{s} = 3.5 MPa. The Young's moduli of cemented soil and steel strand were 200 MPa and 195 GPa, respectively. The parameters of the generalized tri-linear bond-slip model were calibrated based on the mechanical properties of the soil and the inversion analysis for the pullout test results, including s_{e} = 6 mm, s_{p} = 12 mm, τ_{f} = 22 kPa, and

$\eta = 0.1$. The in-situ pullout test results of the single anchors M5 and M15, as well as the second group of the anchor group, were selected to verify the theoretical analysis method. Figure 5 compares the pullout load–displacement responses of the single anchor and the anchor group obtained from in-situ pullout tests and theoretical predictions. The collected measurements of the single anchor presented herein are the average of the test results of anchors M5 and M15 obtained through statistical analysis by Chen et al. [5]. It can be observed that the predicted pullout load–displacement curves match well with the measurements of both single anchor and anchor group. Besides, within the designated testing load range, the pullout displacement of the anchor group was greater than that of the single anchor.

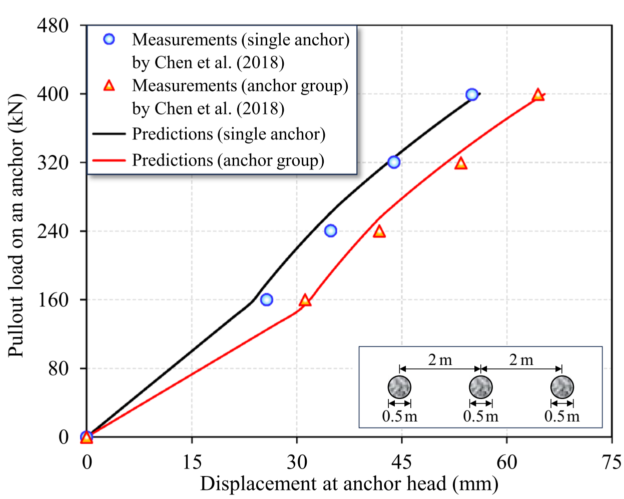

Fig. 5 Comparisons of the pullout load–displacement responses obtained from in-situ tests and theoretical predictions for the large-diameter cemented soil anchor

4.2 Case 2: Laboratory pullout test on wooden anchor group

Li et al. [21] carried out the laboratory pullout test on the wooden anchor group embedded in rammed earthen sites. There were four anchors in the group, arranged in square pattern with spacing distance of 50 cm. All anchors were 6 cm in diameter and 40 cm in anchorage length. The quality proportion of the grouting material was: calcined ginger nuts: quartz sand: water = 1: 1: 0.8. The reinforcement bar was white ash wood, with diameter of 2 cm at the top and 3 cm at the bottom. The diameter of the reinforcement bar was stipulated as 2.5 cm to simplify the theoretical analysis. All four anchors were loaded synchronously using hydraulic jack. The pullout displacement at the heads of all anchors remained equivalent during the entire loading process. The four anchors exhibited the same load–displacement responses owing to their symmetrical arrangement. The remolded loess was filled into the pullout test chamber through layered compaction. The soil mechanical parameters were summarized as: moisture content $w = 14.5\%$, cohesion $c = 20$ kPa, internal friction angle $\varphi = 36°$, Poisson's ratio $\nu_s = 0.3$, unit weight $\gamma = 17.0$ kN m^{-3}, Young's modulus $E_s = 10$ MPa, and shear modulus $G_s = 3.8$ MPa. The mechanical parameters of the grouting material and the white ash wood were summarized as: $E_g = 30$ MPa, $\nu_g = 0.3$, and $E_r = 8.1$ GPa. The parameters of the generalized tri-linear bond-slip model were calibrated based on the mechanical properties of the soil and the inversion analysis for the pullout test results, including $s_e = 4$ mm, $s_p = 24$ mm, $\tau_f = 120$ kPa, and $\eta = -0.6$. Li et al. [21] also conducted numerical simulation for the laboratory pullout test. As evidenced in Fig. 6, the theoretically calculated pullout load–displacement curve exhibits good consistency with both measurements and numerical simulations. It proves the efficacy and accuracy of the above-developed theoretical analysis method.

4.3 Case 3: In-situ pullout test on the anchor group used in transmission line foundation

Zhang et al. [47] conducted the in-situ full-scale pullout tests on the single anchor and the anchor group used in the foundation of transmission line towers. The in-situ pullout test results of the single anchor numbered DM2 and the anchor group numbered QM4-2 were selected to verify the theoretical analysis method. The anchors were all 130 mm in diameter, 4 m in anchorage length, and 0.4 m in free length. There were four anchors in the group, arranged in square pattern with spacing distance of 60 cm. The hot-rolled steel bar with grade of HRB400 was utilized as the reinforcement bar, the dimension of which is 32 mm. The grouting material was fine stone concrete with strength grade of C30. The Young's moduli of grouting body and steel bar were 30 GPa and 200 GPa, respectively. The anchorage segment was mainly located in the medium weathered granite. The mechanical parameters of the surrounding rock were summarized as: Young's modulus $E_s = 9.04$ GPa, Poisson's ratio $\nu_s = 0.26$, cohesion $c = 11.3$ MPa, internal friction angle $\varphi = 50°$, and shear modulus $G_s = 3.58$ GPa. All anchors in the group were connected in parallel to a foundation platform, and were loaded simultaneously using a hydraulic jack. The total pullout load and total displacement at the top of the anchor group were monitored during the entire loading process. The parameters of the generalized tri-linear bond-slip model were calibrated based on the mechanical properties of the surrounding rock and the inversion analysis for the pullout test results, including $s_e = 1.5$ mm, $s_p = 8$ mm, $\tau_f = 210$ kPa, and $\eta = -0.4$. The bond-slip model employed

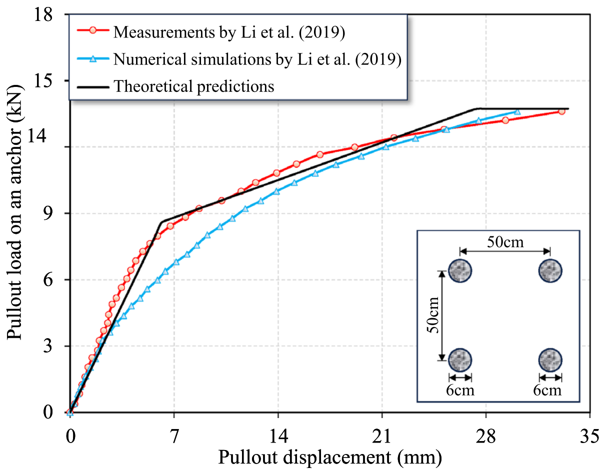

Fig. 6 Comparison of the pullout load–displacement response obtained from laboratory pullout test, numerical simulation and theoretical prediction for the wooden anchor group

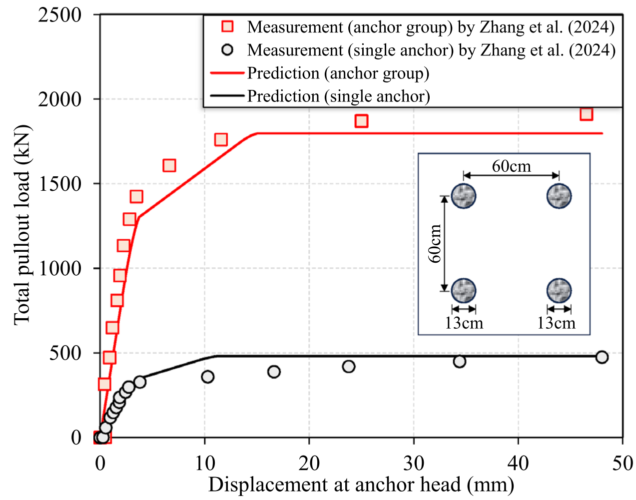

Fig. 7 Comparison of the total pullout load–displacement response obtained from in-situ pullout test and theoretical prediction for the anchor group and the single anchor

to characterize the rock-anchor interface mechanical behavior exhibits the hardening state. Figure 7 compares the total pullout load–displacement responses of the single anchor and the anchor group obtained from in-situ pullout tests and theoretical predictions. The pullout capacities of the single anchor and the anchor group were measured to be 482.3 kN and 1901.1 kN, and were calculated to be 480.3 kN and 1796.3 kN, respectively. The calculation errors are 0.4% and 5.5%, respectively. In general, the results obtained through these two methods exhibit excellent consistency for both single anchor and anchor group. Furthermore, the pullout capacity of each individual anchor within the anchor group is lower than that of a single anchor.

4.4 Case 4: Laboratory physical model test on double anchors

Yang et al. [42] carried out the physical model test on double anchors. The geometric similarity ratio between the model test and the prototype was designed as 1: 15. The anchors in the model tests were all 10 mm in diameter, 200 mm in anchorage length, and 0 m in free length. The model tests were divided into three groups, including single anchor and double anchors with spacing distances of 67 mm and 267 mm. Aluminum wire with dimension of 4 mm was utilized as the reinforcement bar, the Young's modulus of which is 70 GPa. Cement mortar was used as the grouting material, the Young's modulus of which is 20 GPa. Quartz sand, gypsum powder, talc powder, ordinary Portland cement, and water were used to produce the rock-like material around the anchors. The quality ratio of these raw materials was set at 0.78: 0.06: 0.07: 0.01: 0.08. The rock-like material was filled into the model test box in layers, with each layer of 5 cm in thickness. The mechanical parameters of the rock-like material were summarized as: Young's modulus E_s = 28 MPa, Poisson's ratio ν_s = 0.33, cohesion c = 21 kPa, internal friction angle φ = 26°, and shear modulus G_s = 11.2 MPa. The two anchors in the group were connected in parallel to a foundation platform and were loaded simultaneously using a hydraulic jack. The pullout load applied to the anchor head increases by 55 N each time until the anchors fail, which is marked by an unstable pullout displacement. Four strain gauges were attached to each anchor along the anchorage segment with spacing distance of 67 mm. The objective of this configuration was to determine the stress distributions. The parameters of the bond-slip model (Eq. 20) were calibrated based on the mechanical properties of the rock-like material and the inversion analysis for the pullout test results, including s_e = 0.4 mm, s_{p-} = 1.0 mm, τ_f = 60 kPa, and η = -0.3. As evidenced in Fig. 8, the calculated pullout load–displacement curves agree generally well with the testing results for the single anchor and the double anchors with different spacing distances. In this case, the calculated bearing capacity of the double anchors decreased by 113.4 N (11.8%) when their spacing distance was reduced from 267 to 67 mm.

As shown in Fig. 9, the theoretically predicted axial force distributions under different pullout loads demonstrate reasonable agreement with measurements for both single anchor and double anchors. Even so, the discrepancies between the predictions and the measurements grow as the pullout load increases. It may be ascribed to the insufficiently detailed modelling of the anchor group effect in theoretical analysis. Specifically, the group effect was considered through the method of simple linear superposition. Perhaps it cannot adequately reflect the complex and nonlinear interactions between adjacent anchors. It can be seen from Fig. 9a and c that the axial forces measured at the anchor head ($z = 0$ cm) were significantly higher. The phenomenon may be attributed to the fact that this position corresponds to the initial end of the anchorage segment, where the reinforcement bar is not sufficiently bonded with the grouting material or experiences disengagement during the loading process. This may also be a contributing factor to the prediction error. Overall, the predictions are consistent with the measurements. The findings proved the efficacy and accuracy of the above-developed theoretical analysis method.

5 A GWO-based optimal design method for the grouted anchor group

The grey wolf optimization (GWO) algorithm was proposed by Mirjalili et al. [25] as an inspiration from the hunting behavior of grey wolf packs. It is a new type of swarm intelligence optimization algorithm with the merits of simple structure, few adjustable parameters, and easy implementation. Additionally, the GWO algorithm exhibits superior solution accuracy and stability compared to some classical optimization algorithms, such as particle swarm optimization (PSO) [9], genetic algorithm (GA) [41], and ant colony optimization (ACO) [7]. Therefore, the GWO algorithm has been successfully adopted in many fields.

5.1 Mathematical model of GWO algorithm

There is a strict hierarchy system within the gray wolf population. As shown in Fig. 10a, the wolf at the top of the

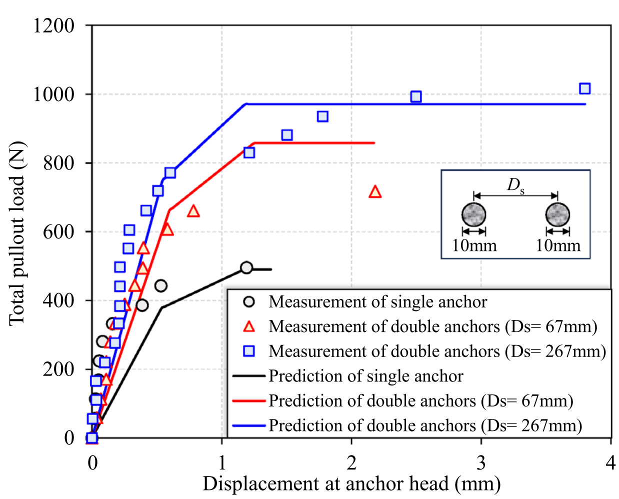

Fig. 8 Comparison of the total pullout load–displacement response obtained from in-situ pullout test and theoretical prediction for the wooden anchor group (measurements from Yang et al. [42])

pyramid is defined as alpha (α). The α wolf is the leader of the entire population and is responsible for making decisions regarding the hunting activity. The wolves at the second and third layers are named beta (β) and delta (δ), respectively. The β wolf assists the α wolf in making decisions, and its leadership position is second only to that of the α wolf. The δ wolf follows the instructions of the α and β wolves. Noteworthy that the α and β wolves will be downgraded to the δ wolf if their adaptability is poor. The ω wolves situated at the bottom of the pyramid are responsible for maintaining the internal relationships within the population.

The GWO algorithm achieves the goal of finding the best solutions through the simulation of the hunting process of the wolf population, which includes tracking, surrounding, chasing, and attacking prey. This process can be summarized mathematically as follows. First, a group of wolves is randomly generated in the designated search area. Then, the three individuals with the best fitness in the population are selected as the α, β, and δ wolves. They were responsible for evaluating the position of the prey, that is, the best solution. Finally, the ω wolves calculate the distances between themselves and the prey, thereby completing the encirclement and capture of the prey (Fig. 10b). The best solution can thus be determined by implementing the aforementioned process. The following is a detailed exposition of the mathematical model for the GWO algorithm.

The encircling behavior of the grey wolves can be mathematically represented by the following equation:

$$\boldsymbol{D} = \left|\boldsymbol{C} \cdot \boldsymbol{X}_{\mathrm{p}}(t) - \boldsymbol{X}(t)\right| \tag{30}$$

$$\boldsymbol{X}(t+1) = \boldsymbol{X}_{\mathrm{p}}(t) - \boldsymbol{A} \cdot \boldsymbol{D} \tag{31}$$

where $\boldsymbol{D}$ denotes the distance between wolf and grey; t denotes the number of positions updating; $\boldsymbol{A}$ and $\boldsymbol{C}$ are random coefficient vectors; $\boldsymbol{X}(t)$ denotes the position vector of the t-th generation of the wolves; $\boldsymbol{X}_{\mathbf{p}}(t)$ denotes the position vector of the grey.

The coefficient vectors $\boldsymbol{A}$ and $\boldsymbol{C}$ can be determined using Eqs. (32) and (33).

$$\boldsymbol{A} = 2\boldsymbol{a} \cdot \boldsymbol{r}_1 - \boldsymbol{a} \tag{32}$$

$$\boldsymbol{C} = 2 \cdot \boldsymbol{r}_2 \tag{33}$$

where $\boldsymbol{a}$ is random factor, which decreases linearly from 2 to 0 during the iterative updating process; $\boldsymbol{r}_1$ and $\boldsymbol{r}_2$ are random vectors, with their values ranging from 0 to 1.

The positions of the wolves are constantly updated during the hunting process. After each update, the positions of the α, β, and δ wolves with the best fitness values are saved. Subsequently, based on the positions of α, β, and δ wolves, the ω wolves update their positions in the next round until the best solution is determined or the specified

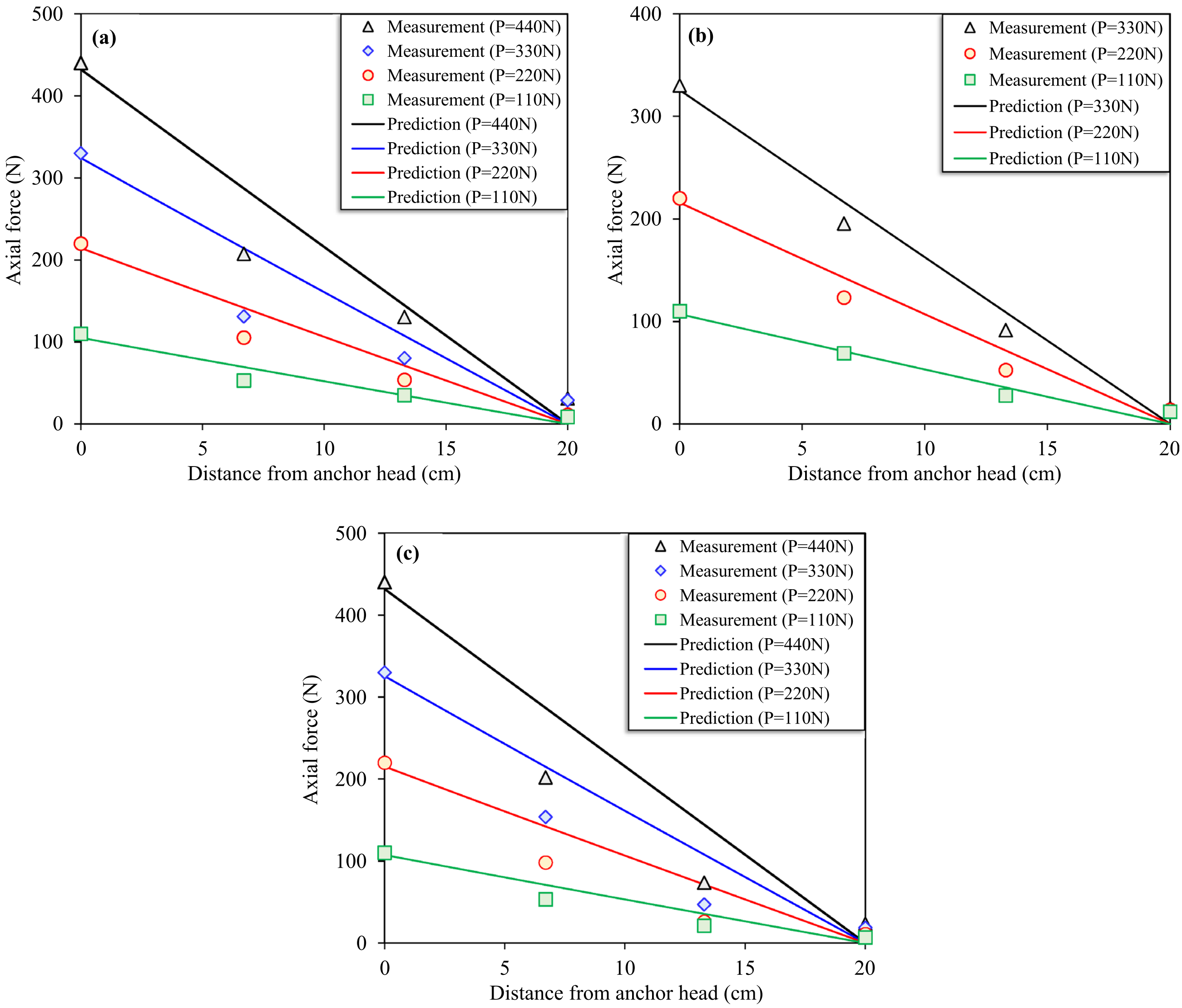

Fig. 9 Comparisons of the predicted axial force distributions under different pullout loads with the in-situ test results (measurements from Yang et al. [42]): **a** single anchor; **b** double anchors (D_s = 67 mm); **c** double anchors (D_s = 267 mm)

number of updates is achieved. The following equation can mathematically express this process:

$$\begin{cases} \boldsymbol{D}_\alpha = |\boldsymbol{C}_1 \cdot \boldsymbol{X}_\alpha(t) - \boldsymbol{X}(t)| \\ \boldsymbol{D}_\beta = |\boldsymbol{C}_2 \cdot \boldsymbol{X}_\beta(t) - \boldsymbol{X}(t)| \\ \boldsymbol{D}_\delta = |\boldsymbol{C}_3 \cdot \boldsymbol{X}_\delta(t) - \boldsymbol{X}(t)| \end{cases} \tag{34}$$

$$\begin{cases} \boldsymbol{X}_1 = \boldsymbol{X}_\alpha(t) - \boldsymbol{A}_1 \cdot \boldsymbol{D}_\alpha \\ \boldsymbol{X}_2 = \boldsymbol{X}_\beta(t) - \boldsymbol{A}_2 \cdot \boldsymbol{D}_\beta \\ \boldsymbol{X}_3 = \boldsymbol{X}_\delta(t) - \boldsymbol{A}_3 \cdot \boldsymbol{D}_\delta \end{cases} \tag{35}$$

$$\boldsymbol{X}(t+1) = \frac{\boldsymbol{X}_1 + \boldsymbol{X}_2 + \boldsymbol{X}_3}{3} \tag{36}$$

where $\boldsymbol{D}_\alpha$, $\boldsymbol{D}_\beta$, and $\boldsymbol{D}_\delta$ represent the distances between the ω wolf and the α, β, and δ wolves, respectively; $\boldsymbol{X}_\alpha(t)$, $\boldsymbol{X}_\beta(t)$, and $\boldsymbol{X}_\delta(t)$ represent the position vectors of the α, β, and δ wolves in the t-th round of calculation, respectively; $\boldsymbol{X}(t)$ and $\boldsymbol{X}(t+1)$ are the position vectors of the ω wolf in the current t-th and the $(t+1)$-th rounds of calculation, respectively.

5.2 Objective function and boundary conditions of the optimization model

The objective of optimal design for the anchor group is mainly to minimize the cost while adhering to the established engineering requirements. Therefore, the design parameters that exert the predominant influence on the bearing performance and cost of the anchor group are selected as the optimization variables, including anchorage length L_a, free length L_f, anchor diameter d, spacing distance between adjacent anchors D_s, and diameter of rebar

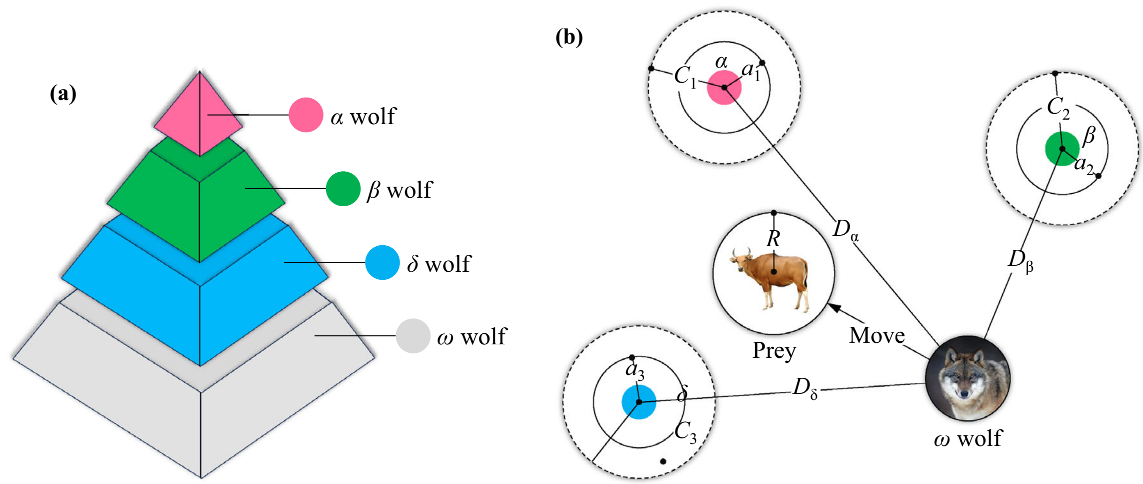

Fig. 10 Schematic diagram of the GWO algorithm: **a** hierarchy system of the grey wolves; **b** position updating path of a wolf

d_r. It is assumed that the design parameters for each anchor in the anchor group are all the same. The total cost $f(\boldsymbol{X})$ of all the anchors within the construction area was defined as the objective function for optimal design. $f(\boldsymbol{X})$ is primarily constituted by three parts: the construction cost f_1, the cost of grouting material f_2, and the cost of rebars and anchorage devices f_3.

$$f(\boldsymbol{X}) = f_1 + f_2 + f_3 \tag{37}$$

where

$$\begin{cases} f_1 = c_1(L_a + L_f)n_a \\ f_2 = c_2V_m n_a = \dfrac{c_2\pi(d^2 - d_r^2)L_a n_a}{4} \\ f_3 = (c_3 m_r + c_4)n_a = \left[\dfrac{c_3\rho_r\pi d_r^2(L_a + L_f)}{4} + c_4\right]n_a \end{cases} \tag{38}$$

where c_1 is the construction cost per meter; c_2 is the cost per cubic meter of grouting material; c_3 is the cost of a unit weight of the rebar; c_4 is the base price of the anchorage device; V_m is the grouting volume of one anchor; m_r is the quality of the rebar for one anchor; n_a is the number of all anchors in the construction region, $n_a \approx \lceil A_t/A_s \rceil$; A_t is the total area of the construction region; A_s is the reinforcement area for each individual anchor, which can be calculated by Eq. (39), as shown in Fig. 11; ρ_r and d_r are the density and diameter of the rebar, respectively.

$$A_s = \begin{cases} D_s^2, & \text{Square layout} \\ \dfrac{\sqrt{3}}{2}D_s^2, & \text{Equilateral triangle layout} \end{cases} \tag{39}$$

The bearing capacity of the anchor group must be adequate to ensure the safety of the engineering structure. In addition, the feasible ranges for all optimization variables should be restricted to facilitate the construction of grouted anchors. Therefore, the following conditions were stipulated in the proposed optimization model.

$$\begin{cases} g_1(\boldsymbol{X}) = [T_f] - \dfrac{T_f}{K_s} \le 0 \\ g_2(\boldsymbol{X}) = T_f - \sigma_f A_r \le 0 \\ g_3(\boldsymbol{X}) = d - D_s \le 0 \\ g_4(\boldsymbol{X}) = d - 0.2 \le 0 \\ g_5(\boldsymbol{X}) = 0.1 - d \le 0 \end{cases} \tag{40}$$

where T_f is the ultimate pullout capacity, which can be determined through the developed theoretical analysis method; $[T_f]$ is the pullout load applied to one anchor, $[T_f] = pA_s$; p is the load per square meter; K_s is safety factor; σ_f is the tensile strength of rebar.

The optimal design model for the grouted anchor group is expressed as:

$$\begin{cases} \boldsymbol{X} = [x_1, x_2, x_3, x_4, x_5]^T = [L_a, L_f, d, D_s, d_r]^T \\ \min f(\boldsymbol{X}) = f_1 + f_2 + f_3 \\ \text{s.t.}\, g_i(\boldsymbol{X}) \le 0, \qquad i = 1, \ldots, 5 \end{cases} \tag{41}$$

5.3 Optimal design procedures of the grouted anchor group

The GWO algorithm was utilized to search for the global best solution to the aforementioned model, the procedure of which was illustrated in Fig. 12. The details were elaborated as follows.

Step (1): Specify the ranges of all optimization variables $\boldsymbol{X}$ for the anchor group. Assign values to the mechanical

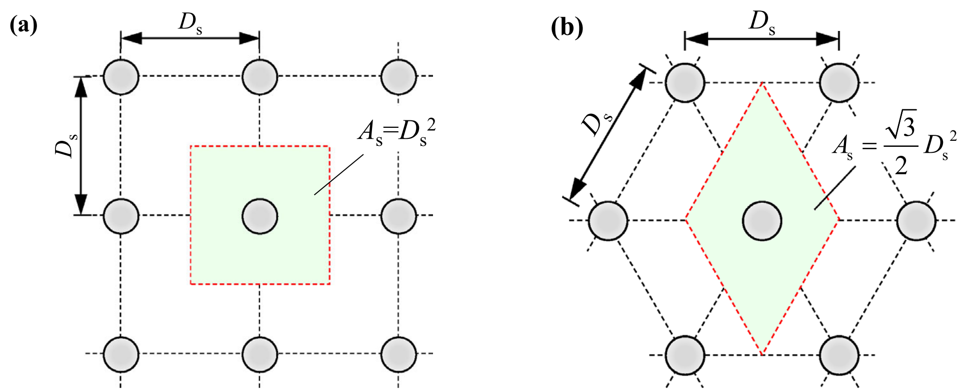

Fig. 11 Layout of the anchor group and the reinforcement area for one anchor: **a** square layout; **b** equilateral triangle layout

parameters of the soil, grout, rebar, and soil–anchor interface. Clarify the design requirements, such as the total area of the construction region A_t, the load per square meter p, and the safety factor K_s. The base prices for construction and various materials are stipulated. The objective function $f(\boldsymbol{X})$ and constraint conditions $g(\boldsymbol{X})$ for the optimal design can thus be established, as shown in Eqs. (37) and (40).

Step (2): Define the number of gray wolves N in the population and the maximum number of calculations t_{max}. Initialize the random factor a, random coefficient vectors $\boldsymbol{A}$ and $\boldsymbol{C}$. In this study, $N = 30$ and $t_{max} = 100$. The initial population of grey wolves is further generated based on the constraint conditions.

Step (3): Search for the best design parameters of the anchor group through the GWO algorithm. Specifically, the fitness values of all the gray wolves are calculated by Eq. (37). The fitness values and positions of the α, β, and δ wolves are determined according to the calculation results. The random factor a, random coefficient vectors $\boldsymbol{A}$ and $\boldsymbol{C}$ are updated, and the new positions of ω wolves can further be determined by Eq. (36). In the current round of calculation, if the constraint conditions (Eq. 40) cannot be satisfied, the random coefficient vectors $\boldsymbol{A}$ and $\boldsymbol{C}$ should be re-updated to obtain the suitable positions of ω wolves. Record the fitness values and positions of the α wolf after each round of updating.

Step (4): Repeat step (3) until the maximum number of calculations t_{max} is achieved. The final fitness value of α wolf represents the lowest cost of the anchor group that meets all the design requirements, and its corresponding position is the best design parameters. Noteworthy that adjustments to the obtained best design parameter may be necessary to facilitate the construction of grouted anchors.

6 Case study on the optimal design of grouted anchor group employed in anti-floating engineering

The World Computing Changsha Intelligent Valley project is located in Changsha City, Hunan Province, China. The E12 plot was earmarked for the construction of eight high-rise office buildings. In this area, the groundwater level was observed to be relatively high, prompting the utilization of ground anchors to mitigate the risk of buildings floating. A rectangular field measuring 228 m in length and 52 m in width is situated between the T4 and T8 high-rise office buildings. The total area of this field is 11,856 m^2. There is 64.6 m in ground elevation, 61.5 m in average waterproof elevation for anti-floating, and 54.9 m in average elevation of the basement. Subsequent to the deduction of the building's inherent mass, the anti-floating force provided by the anchors is approximately 50 kN/m^2. The foundation strata are mainly composed of miscellaneous fill, silty clay, fully weathered granite, and strongly weathered granite, the basic properties of which were summarized in Table 1.

The anti-floating anchors designed in original plan were 200 mm in diameter, approximately 2.2 m in spacing distance, and approximately 12 m in average anchorage length. Besides, the characteristic value of pullout capacity for one anchor was designed as 270 kN, and the safety factor was 2.0. The anchorage segments were mainly embedded in the fully weathered granite. The Young's

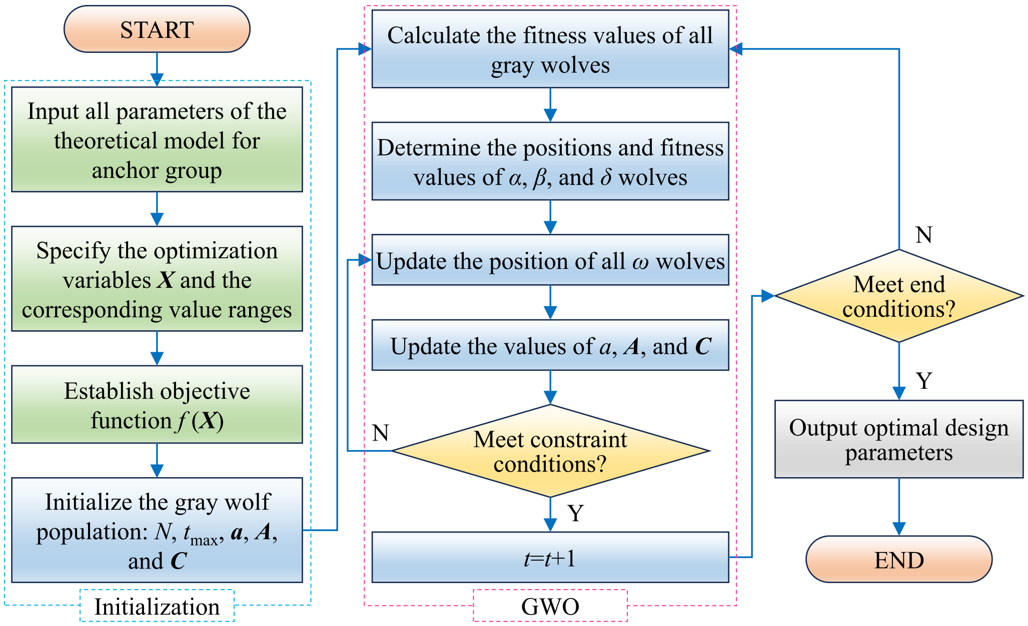

Fig. 12 Procedures for searching the best design parameters of the anchor group using the GWO algorithm

modulus and the Poisson's ratio of this layer of soil are 80 MPa and 0.3, respectively. The grouting material is a specialized cement paste with the mark of M35, water-cement ratio of 0.38, elastic modulus of 25 GPa, and Poisson's ratio of 0.22. Three low-relaxation steel strands, each with a diameter of 15.2 mm, were used as the reinforcement bar. The steel strand is 195 GPa in elastic modulus and 1890 MPa in tensile strength. Based on the mechanical properties of the surrounding soil, the four parameters of the generalized tri-linear bond-slip model were calibrated as: $s_e = 4.2$ mm, $s_p = 7.6$ mm, $\tau_{f-} = 105$ kPa, and $\eta = 0.25$. The ultimate pullout capacity of an individual anchor was measured to be 600 kN through in-situ pullout test, and the theoretical calculation of that is 608 kN. The discrepancy between the two results is merely 1.3%, indicating the reliability of the proposed theoretical model as well as its parameters.

The unit prices for construction and various materials were determined based on the local price conditions, which were summarized as: $c_1 = 58$ ¥/m, $c_2 = 850$ ¥/m^3, $c_3 = 4.5$ ¥/kg, and $c_4 = 78$ ¥/piece. Approximately 2,450 anti-floating anchors were needed for this area in the original design, and the corresponding total cost was almost ¥3.305 M. Hereinto, the construction cost for anchor hole drilling f_1 was ¥1.70 M, the cost of grouting material f_2 was ¥0.77 M, and the cost of rebars and anchorage devices f_3 was ¥0.83 M. The original design of the anti-floating anchor group was then optimized through the implementation of the developed GWO-based optimal design method. The PSO algorithm was also employed in the optimal design to facilitate comparison. The parameters of the PSO algorithm were specified as: population size $N = 30$, inertia weight $w = 0.5$, self-learning factor $c_1 = 0.5$, group learning factor $c_2 = 0.5$, and maximum number of calculations $t_{max} = 100$. The free length and the diameter of the steel strands are consistent with the original design.

Table 2 summarizes the design parameters and total costs of the anchor group before and after optimization. Figure 13 depicts the cost breakdown of the original and the optimized designs. The goal of significantly reducing the project cost while meeting the design requirements is

Table 1 Basic properties of each layer of soil within the construction area

	Average thickness (m)	Unit weight (kN·m^{-3})	Internal friction angle (°)	Cohesive force (kPa)	Plastic index (%)	SPT
Miscellaneous fill	3.1	19.5	10	10	/	/
Silty clay	1.4	19.9	15	31	16.6	18
Fully weathered granite	21.9	19.3	16	32	16.5	33
Strongly weathered granite	/	23.2	28	42	/	> 50

successfully achieved through the implementation of the GWO-based optimal design method. In instances where anchors are arranged in square layout, the GWO-based optimal design reduces the total cost by 27.6% compared to the original design. Besides, it is more cost-effective to arrange the anchors in square than equilateral triangle. For example, the total cost of the square layout is ¥335 K less than that of the equilateral triangle layout for the designs obtained by the GWO-based optimum method. It can also be observed from Fig. 13 that the construction cost f_1 is the highest, accounting for approximately 50% of the total cost, and following that are the material costs of steel strands and grouting material.

The calculation convergence speeds of the GWO and PSO algorithms are comparable, and both can achieve convergence within 20 iterative calculations, as shown in Fig. 14. However, a comparison of the optimal design based on the GWO algorithm with that of the PSO algorithm revealed that the former can yield a lower cost. When the anchors are arranged in the square and equilateral triangle layouts, the total costs of the design schemes obtained by PSO algorithm are ¥83 K and ¥87 K much more than those obtained by GWO algorithm, respectively. This can be attributed to the inherent limitations of the PSO algorithm, which is prone to converging on a local optimal solution rather than the global optimal solution. Overall, the findings indicate that the GWO algorithm is equipped with higher accuracy in searching for the best design parameters for the grouted anchor group.

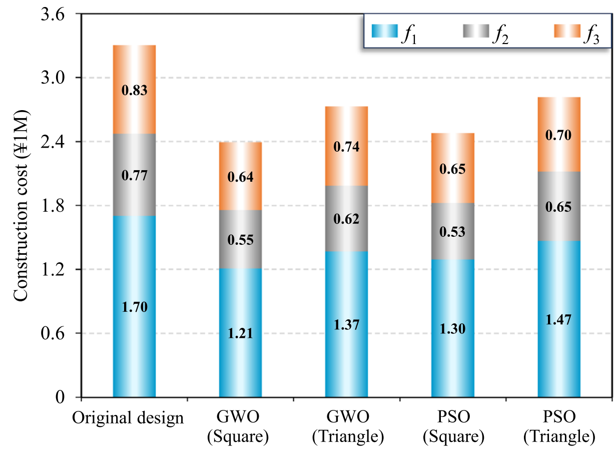

Fig. 13 Cost breakdown of the original and the optimized designs

7 Parametric studies

The spacing distance, anchorage length, and layout method are critical design parameters for the anchor group, as they can significantly influence the bearing performance. Therefore, parametric studies were conducted via the proposed theoretical analysis method to investigate the impacts of those key parameters on the pullout capacity of the grouted anchor group. Except for special instructions, the basic model parameters were set as follows. The anchors were 150 mm in diameter and 12 m in anchorage length. The grouting material was cement mortar with Young's modulus of 20 GPa. The Young's modulus and the Poisson's ratio of the surrounding soil were 80 MPa and 0.33, respectively. The reinforcement bar was steel rebar with diameter of 28 mm and elastic modulus of 195 GPa. The parameters of the bond-slip model were: τ_{f} = 120 kPa, η = 1.0, s_e = 5 mm, and s_p = 45 mm.

7.1 Impact of spacing distance between adjacent anchors

Figure 15 shows the variation of the pullout capacity of an individual anchor within the anchor group with the spacing distance under square and equilateral triangular layouts. The pullout capacity of the anchor increases as the spacing distance increases, yet the increasing rate gradually decreases. In the present case, the increase in spacing distance exerts a negligible impact on the improvement of the pullout capacity once the ratio of the spacing distance to the diameter D_s/d exceeds approximately 18. Furthermore, the pullout capacity of the anchor group is marginally higher in the regular triangular layout compared to the square layout, in particular for the case where the spacing distance is relatively small.

Table 2 Comparison of the design parameters and total costs of the anchor group between the original and the optimized plans

	Original design	GWO (square)	GWO (triangle)	PSO (square)	PSO (triangle)
Anchor diameter d (m)	0.20	0.20	0.20	0.19	0.20
Spacing distance D_s (m)	2.20	2.25	2.18	2.35	2.70
Anchorage length L_a (m)	12.00	8.90	8.20	10.36	13.60
Rebar diameter d_r (m)	0.028	0.028	0.028	0.028	0.028
Free length L_f (m)	0	0	0	0	0
Construction cost (¥1 M)	3.305	2.394	2.729	2.477	2.816

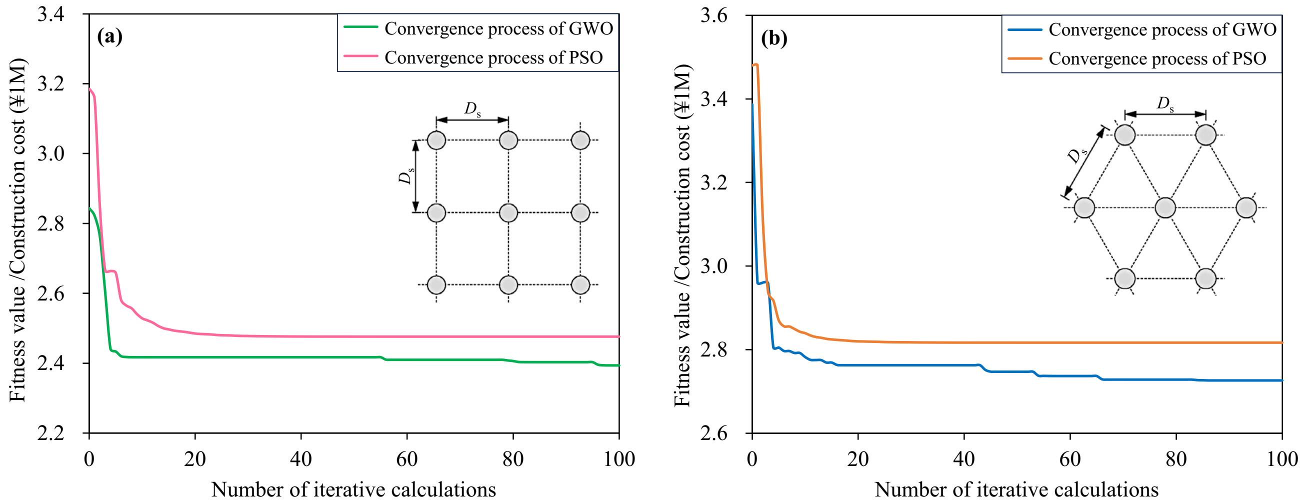

Fig. 14 Comparison of the calculation convergence speeds between the GWO and PSO algorithms: **a** square layout; **b** equilateral triangle layout

7.2 Impact of anchorage length

The variations of the pullout capacity with the anchorage length under different interface softening coefficients were illustrated in Fig. 16. It can be observed that the pullout capacity of an individual anchor within the anchor group increases with increasing anchorage length. However, there will be a critical value for the anchorage length L_a when the interface softening coefficient η exceeds 0.7, which is designated as the effective anchorage length L_a^*. For example, the effective anchorage length L_a^* is approximately 12 m when $\eta = 0.7$. The increase in pullout capacity will be very small when L_a exceeds L_a^*. The interface softening coefficient η is generally large for the anchors that are embedded in pan soil or soft rock, indicating that the soil–anchor interface exhibits significant softening behaviors. In such geological conditions, it is unreasonable to enhance the bearing capacity of the anchor group by excessively increasing the anchorage length.

As demonstrated in Fig. 17, the spacing distance exerts minimal influence on the pullout capacity of the anchor group when the anchorage length is relatively short. As the anchorage length increases, particularly when it exceeds 6 m, the influence of spacing distance on the pullout capacity becomes more significant. Therefore, the reduction in bearing capacity resulting from the group effect of anchors necessitates meticulous consideration if the anchorage length is relatively long and the spacing distance between adjacent anchors is relatively small.

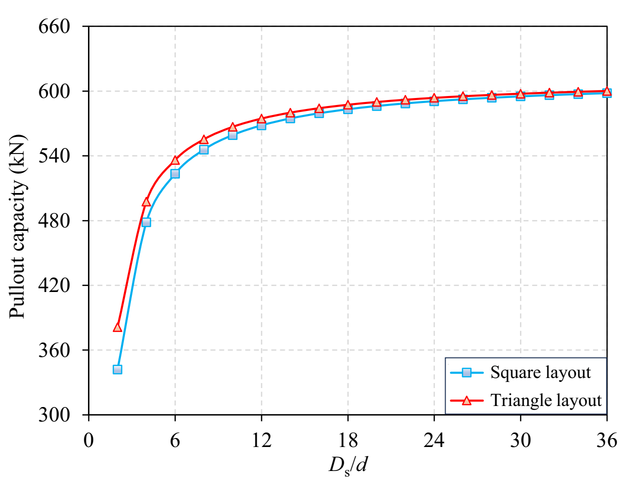

Fig. 15 The pullout capacity of an individual anchor within the anchor group versus the spacing distance under square and equilateral triangular layouts (L_a = 12 m, η = 0.2)

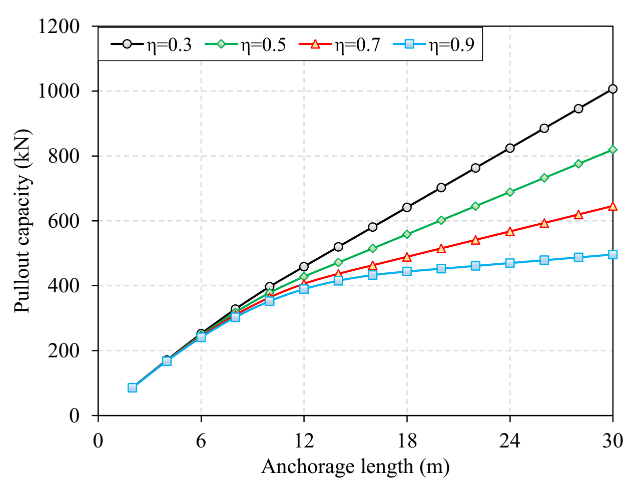

Fig. 16 Variation of the pullout capacity with the anchorage length under different interface softening coefficients

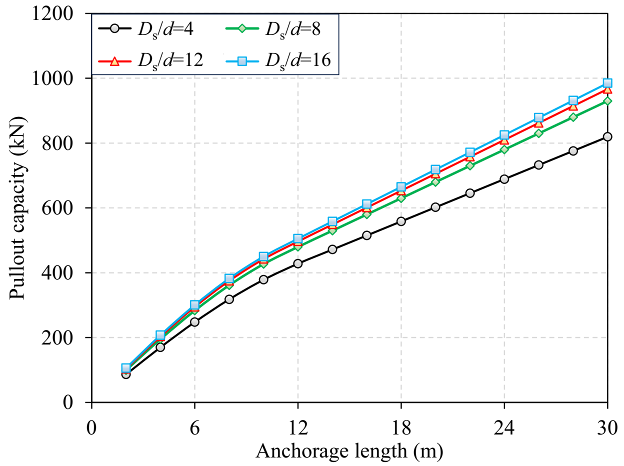

Fig. 17 Variation of the pullout capacity with the anchorage length under different spacing distances

8 Summary and conclusions

A theoretical analysis method for the pullout behaviors of grouted anchor group was proposed in this paper, in which the group effect was specially considered by integrating load-transfer theory and shear deformation method. The predicted pullout load–displacement responses and axial force distributions were compared with the results from four separate in-situ and laboratory pullout tests for the single anchor and anchor group. Based on the GWO algorithm, a novel optimal design method driven by the lowest cost was developed for the anchor group. The impacts of spacing distance, anchorage length, and layout form on the pullout capacity of the anchor group were investigated by parametric studies. The following conclusions can be deduced:

(1) The theoretically predicted pullout load–displacement curves and axial force distributions under different loads were generally in good agreement with the in-situ and laboratory pullout test results. The findings confirmed the efficacy and accuracy of the proposed theoretical analysis method for the pullout behaviors of the grouted anchor group.

(2) Due to the interaction between adjacent anchors (group effect), the pullout capacity of each individual anchor within the anchor group is lower than that of a single anchor, yet the pullout displacement is greater. The reduction in bearing capacity resulting from the group effect necessitates meticulous consideration if the anchorage length is relatively long and the spacing distance between adjacent anchors is relatively small, especially when the ratio of the spacing distance to the anchor diameter is less than 18.

(3) The implementation of the GWO-based optimal design method can substantially reduce the project cost while meeting the design requirements for the anchor group. In comparison with the PSO algorithm, the GWO algorithm is more accurate in searching for the best design parameters.

(4) The pullout capacity of the anchor group is marginally higher in the regular triangular layout compared to the square layout, particularly for the case where the spacing distance between adjacent anchors is relatively small.

In summary, the present study offered a new theoretical method for analyzing the pullout responses of the grouted anchor group and optimizing its design parameters. The findings can provide theoretical guidance for the bearing performance evaluation of the anchor group, and can also facilitate the cost-effective optimization design. However, in the actual anchorage engineering, the layout of anchor group may not be regular, and the design parameters may exhibit variability across different anchors, such as anchorage length, free length, anchor diameter, spacing distance, etc. The anchors within the group will exhibit remarkably intricate load–displacement behavior under these conditions. In light of the aforementioned challenges, new approaches and theories are imperative for addressing the issues associated with the bearing performance analysis and design optimization of the grouted anchor group.

Acknowledgements This research was sponsored by the Shandong Provincial Natural Science Foundation (No. ZR2024QE444), the National Natural Science Foundation of China (No. 52278349), the Hunan Provincial Key Laboratory for Big Data Smart Application of Natural Disaster Risks Survey of Highway Engineering (No. BNH2024KFA03). The authors appreciate their financial support.

Data availability All data, models, and codes generated or used during the study are available from the corresponding author upon reasonable request.

Declarations

Conflict of interest The authors declare that they have no known competing financial interests or personal relationships that could have appeared to influence the work reported in this paper.

References

1. Akis E, Bakir BS, Yilmaz MT (2024) The effect of group behavior on the pull-out capacity of model soil nails in high plasticity clay. Innov Infrastruct Solut 9:215. https://doi.org/10.1007/s41062-024-01520-7
2. Chan CM, Zhang LM, Ng JTM (2009) Optimization of pile groups using hybrid genetic algorithms. J Geotech Geoenviron Eng 135(4):497–505. https://doi.org/10.1061/(ASCE)1090-0241(2009)135:4(497)

3. Chen CF, Mao FS, Zhang GB, Huang J, Zornberg JG, Liang X, Chen J (2021) Settlement-based cost optimization of geogrid-reinforced pile-supported foundation. Geosynth Int 28(5):541–557. https://doi.org/10.1680/jgein.21.00002
4. Chen CF, Zhu SM, Zhang GB, Morsy AM, Zornberg JG, Mao FS (2022) A generalized load-transfer modelling framework for tensioned anchors integrating adhesion-friction-based interface model. Int J Geomech 22(5):04022036. https://doi.org/10.1061/(ASCE)GM.1943-5622.0002338
5. Chen J, Liang WP, Ying HW (2018) Experimental and numerical research on proper interval of large diameter soil–cement anchor cables. Rock Soil Mech 39(S2):374–380
6. Chen WB, Hong CY, Chen XS, Luo GB, Su D (2023) Comparative analysis of anchor cables in pullout tests using distributed fiber optic sensors. Can Geotech J 60:1861–1876. https://doi.org/10.1139/cgj-2022-0455
7. Dorigo M, Blum C (2005) Ant colony optimization theory: a survey. Theor Comput Sci 344:243–278. https://doi.org/10.1016/j.tcs.2005.05.020
8. Fu WG, Zou JF, Huang K (2021) Overview of research on recycled anchor technology. Chin J Undergr Space Eng 17(S1):512–522
9. Gad AG (2022) Particle swarm optimization algorithm and its applications: a systematic review. Arch Computat Methods Eng 29:2531–2561. https://doi.org/10.1007/s11831-021-09694-4
10. Gong ZY, Ouyang HR, Dai GL, Chen XS (2025) A theoretical analysis method for stiffened deep cement mixing (SDCM) pile groups under vertical load in layer soils. Comput Geotech 183:107211. https://doi.org/10.1016/j.compgeo.2025.107211
11. Guo X, Pham TA, Dias D (2023) Multi-objective optimization of geosynthetic-reinforced and pile-supported embankments. Acta Geotech 18:3783–3798. https://doi.org/10.1007/s11440-022-01782-4
12. Hanna A, Ghaly A (1994) Ultimate pullout resistance of groups of vertical anchors. Can Geotech J 31(5):673–682. https://doi.org/10.1139/t94-079
13. Hong CY, Yin JH, Zhou WH, Pei HF (2012) Analytical study on progressive pullout behavior of a soil nail. J Geotech Geoenviron Eng 138(4):500–507. https://doi.org/10.1061/(ASCE)GT.1943-5606.0000610
14. Hong YS, Wu CS, Yang SH (2003) Pullout resistance of single and double nails in a model sandbox. Can Geotech J 40:1039–1047. https://doi.org/10.1139/t03-048
15. Hu JL, Chen CF (2010) Displacement of anchor groups with consideration of reinforcement effect. J Railw Sci Eng 7(3):55–59
16. Huang Y, He ZY, Yashima A, Chen ZY, Li CX (2022) Multi-objective optimization design of pile-anchor structures for slopes based on reliability theory considering the spatial variability of soil properties. Comput Geotech 147:104751. https://doi.org/10.1016/j.compgeo.2022.104751
17. Kong C, Yang T, Xiao M, Yuan QT (2023) Numerical simulation of fully grouted rock bolts with or without faceplates based on the tri-linear bond-slip model. Constr Build Mater 367:130288. https://doi.org/10.1016/j.conbuildmat.2022.130288
18. Kou HL, Guo W, Zhang MY (2015) Pullout performance of GFRP anti-floating anchor in weathered soil. Tunn Undergr Space Technol 49:408–416. https://doi.org/10.1016/j.tust.2015.06.001
19. Lee SW, Kim TS, Sim BK, Kim JS, Lee IM (2012) Effect of pressurized grouting on pullout resistance and group efficiency of compression ground anchor. Can Geotech J 49(8):939–953. https://doi.org/10.1139/t2012-059
20. Li C, Stillborg B (1999) Analytical models for rock bolts. Int J Rock Mech Min Sci 36(8):1013–1029. https://doi.org/10.1016/S1365-1609(99)00064-7
21. Li JF, Zhang JK, Wang N, Zhao LY, Guo QL (2019) Physical model test on working mechanisms of an anchor group system with four wood bolts in rammed earthen sites. Chin J Rock Mech Eng 38(11):2321–2331
22. Liu XM, Wang JQ, Huang J, Jiang HW (2017) Full-scale pullout tests and analyses of ground anchors in rocks under ultimate load conditions. Eng Geol 228:1–10. https://doi.org/10.1016/j.enggeo.2017.07.004
23. Maleki J, Pak A, Yousefi M, Aghakhani N (2022) A comprehensive FE study for design of anchored wall systems for deep excavations. Tunn Undergr Space Technol 122:104340. https://doi.org/10.1016/j.tust.2021.104340
24. Martín LB, Tijani M, Hadj-Hassen F (2011) A new analytical solution to the mechanical behaviour of fully grouted rockbolts subjected to pull-out tests. Constr Build Mater 25(2):749–755. https://doi.org/10.1016/j.conbuildmat.2010.07.011
25. Mirjalili S, Mirjalili SM, Lewis A (2014) Grey wolf optimizer. Adv Eng Softw 69:46–61. https://doi.org/10.1016/j.advengsoft.2013.12.007
26. Ozturk M (2013) Prediction of tensile capacity of adhesive anchors using neural networks. Sci Eng Compos Mater 20(1):95–104. https://doi.org/10.1515/secm-2012-0059
27. Pan XG, Jia JQ (2025) Time-dependent system reliability analysis of anchor-reinforced slopes based on surrogate models. Comput Geotech 184:107257. https://doi.org/10.1016/j.compgeo.2025.107257
28. Pang YS, Liu HL, Ke JW, Chen ZY (2009) Effects of the new type of recoverable anchor groups with different disposing spacings. J Hohai Univ Nat Sci 37(6):685–690
29. Phutthananon C, Jongpradist P, Jongpradist P, Dias D, Jamsawang P, Bergado DT (2021) Performance-based design optimization of embankments resting on soft soil improved with T-shaped and conventional DCM columns. Acta Geotech 16:3301–3326. https://doi.org/10.1007/s11440-021-01258-x
30. Poulos HG (1968) Analysis of the settlement of pile groups. Géotechnique 18(4):449–471. https://doi.org/10.1680/geot.1968.18.4.449
31. Rajwar K, Deep K, Das S (2023) An exhaustive review of the metaheuristic algorithms for search and optimization: taxonomy, applications, and open challenges. Artif Intell Rev 56:13187–13257. https://doi.org/10.1007/s10462-023-10470-y
32. Randolph MF, Wroth CP (1978) Analysis of deformation of vertically loaded piles. J Geotech Eng Div 104(12):1465–1488. https://doi.org/10.1061/AJGEB6.0000729
33. Ren FF, Yang ZJ, Chen JF, Chen WW (2010) An analytical analysis of the full-range behaviour of grouted rockbolts based on a tri-linear bond-slip model. Constr Build Mater 24:361–370. https://doi.org/10.1016/j.conbuildmat.2009.08.021
34. Shin GB, Jo BH, Kim SR, Chung CK, Baek SH (2023) Field study on behavior of load distributive compression anchor installed in weathered rock and soft rock. Can Geotech J 60:1895–1908. https://doi.org/10.1139/cgj-2022-0384
35. Su LJ, Chan TCF, Yin JH, Shiu YK, Chiu SL (2008) Influence of overburden pressure on soil–nail pullout resistance in a compacted fill. J Geotech Geoenviron Eng 134:1339–1347. https://doi.org/10.1061/(ASCE)1090-0241(2008)134:9(1339)
36. Sun HL, Lu W, Zhao D, Li DB (2024) Analytical method for interfacial slip failure processes based on UFL bond-slip model: study of grout/soil anchorage interfaces in earthen sites. Comput Geotech 176:106778. https://doi.org/10.1016/j.compgeo.2024.106778
37. Sun JP, Dong PT, Yu TT (2024) Assessing stability of 3D slopes reinforced with prestressed anchor cables considering strength reserve. Comput Geotech 174:106596. https://doi.org/10.1016/j.compgeo.2024.106596

38. Tan SA, Ooi PH, Park TS, Cheang WL (2008) Rapid pullout test of soil nail. J Geotech Geoenviron Eng 134(9):1327–1338. https://doi.org/10.1061/(ASCE)1090-0241(2008)134:9(1327)
39. Tao ZG, Lei XT, Liu KY, Zhang RX, Fan XW, Cai MJ (2025) A model test investigation on prestressed anchor cable support for the Haidong fault tunnel. Tunn Undergr Space Technol 158:106396. https://doi.org/10.1016/j.tust.2025.106396
40. Wang XJ, Zhang X (2022) Experimental and theoretical research on the bearing mechanism of group anchors in sand. Geofluids 2022:1–14. https://doi.org/10.1155/2022/6448589
41. Whitley D (1994) A genetic algorithm tutorial. Stat Comput 4:65–85. https://doi.org/10.1007/BF00175354
42. Yang KC, Wu SG, Liao HC, Zhang H (2023) Mechanism analysis and model test research on double anchor rods. Rock Soil Mech 44(S):495–503. https://doi.org/10.16285/j.rsm.2022.1226
43. Zhang GB, Luo X, Li SQ, Deng LT, Liu YK, Wang ZN, Li ZB, Li MD, Xu CJ (2026) Interface characterization of ground anchors embedded in soybean urease-induced carbonate precipitation-stabilized soils. Acta Geotech. https://doi.org/10.1007/s11440-026-03009-2
44. Zhang QQ, Zhang ZM, He JY (2010) A simplified approach for settlement analysis of single pile and pile groups considering interaction between identical piles in multilayered soils. Comput Geotech 37:969–976. https://doi.org/10.1016/j.compgeo.2010.08.003
45. Zhang S, Liu W, Ye XY, Li Y, Shi YF, Wang SY (2023) Experimental study of the improvement of surrounding soils due to the grouting with a geotextile. Acta Geotech 18:5011–5027. https://doi.org/10.1007/s11440-023-01855-y
46. Zhou WH, Yin JH, Hong CY (2011) Finite element modelling of pullout testing on a soil nail in a pullout box under different overburden and grouting pressures. Can Geotech J 48:557–567. https://doi.org/10.1139/t10-086
47. Zhang WX, Cui Q, Qiu HC, Lu Z, Xi BL, Zhang ZH (2024) Onsite full-scale test research for difference of anti-pull bearing characteristics between single anchor and group anchors foundation of transmission lines. Bull Geol Sci Technol 43(6):114–124. https://doi.org/10.19509/j.cnki.dzkq.tb20240221
48. Zhu HH, Yin JH, Yeung AT, Jin W (2011) Field pullout testing and performance evaluation of GFRP soil nails. J Geotech Geoenviron Eng 137(7):633–642. https://doi.org/10.1061/(ASCE)GT.1943-5606.0000457
49. Zhu SM, Chen CF, Cai H, Mao FS (2022) Analytical modeling for the load-transfer behavior of stiffened deep cement mixing (SDCM) pile with rigid cap in layer soils. Comput Geotech 144:104618. https://doi.org/10.1016/j.compgeo.2021.104618
50. Zhu SM, Chen CF, Mao FS, Cai H (2021) Application of disturbed state concept for load-transfer modeling of recoverable anchors in layer soils. Comput Geotech 137:104292. https://doi.org/10.1016/j.compgeo.2021.104292
51. Zhu SM, Chen CF, Zhang GB, Du C (2022) Theoretical and experimental investigations of anchoring force loss behavior for prestressed ground anchors. Can Geotech J 59(9):1587–1601. https://doi.org/10.1139/cgj-2021-0220
52. Zhu SM, Chen CF, Zhang GB, Wang MB, Zhang ZW (2024) A theoretical model for the load-transfer analyses of load distributive compression anchor integrating DSC-based interface non-linear model. Constr Build Mater 449:138250. https://doi.org/10.1016/j.conbuildmat.2024.138250